



Free vibration analysis of exponential AFGM beams with general boundary conditions and tip masses

Mohsen Bambaechee¹ · Morteza Jalili Qazizadeh¹ · Omid Movahedian¹

Received: 21 May 2022 / Accepted: 5 October 2022 / Published online: 26 October 2022
© The Author(s), under exclusive licence to Springer Nature Switzerland AG 2022

Abstract

In this paper, the analytical method and design charts for finding the exact solutions to the free transverse vibration of the exponential axially functionally graded material (AFGM) beams with concentrated tip masses and general boundary conditions are presented. According to the derived formulations, the effects of the elastic supports, attached tip masses, and exponential gradient index on the natural frequencies and mode shapes of the AFGM beams with symmetric and asymmetric boundary conditions are investigated. First, by solving the differential equation governing the free vibration of the exponential AFGM Euler–Bernoulli beams, exact solutions are obtained. The material properties of beams are assumed to vary continuously in the axial direction according to the exponential functions. Second, by applying the general boundary conditions, the matrix of constant factors of the beam is derived explicitly. By setting the determinant of this matrix to zero, the natural frequencies of the exponential AFGM beam with the general boundary conditions will be available. In the following, the mode shapes and design charts of the AFGM beams can be obtained. The advantages of the proposed formulations are accuracy, generality, and simplicity in modeling the various boundary conditions. Results show that tip masses, exponential gradient index, and end supports play an influential role in the dynamic behavior of the AFGM beams. Accordingly, the results and design charts presented for the first time are helpful for the proper design and finding the identical frequency of the exponential AFGM beams, exponential non-uniform beams, and uniform beams with different boundary conditions.

Keywords Axially Functionally Graded Material (AFGM) · Free vibration · Exponential law · Tip mass · Boundary conditions

Introduction

Functionally graded materials (FGM) are advanced inhomogeneous materials that due to improving the thermal and mechanical properties of the structure are widely used in engineering structures such as beams and plates. The composite beams made of FGM can be classified into three major classes. The first class involves beams whose material properties vary through the thickness direction and are

more commonly known as FGM beams. The second class includes beams in which material properties change along the axial direction and so-called axially functionally graded material (AFGM) beams. The third class consists of beams whose material properties vary in both axial and thickness directions and are well-known as bi-direction functionally graded material (BDFGM) beams. In this study, the behavior of the second class, i.e., AFGM beams is investigated. However, the non-uniform homogeneous beams can be considered the special case of the axially functionally graded (AFG) beams with constant material and variable geometry (Bambaechee, 2019).

On the other hand, knowing the dynamic behavior of AFGM beams is necessary for the design of these composite beams. In the last decades, the free vibration of FGM beams with the exponential variation of mechanical properties has been investigated widely and is still receiving attention in the literature. Huang and Li, (2010) proposed a new approach for the free vibration of the non-uniform

✉ Mohsen Bambaechee
m.bambaechee@qiet.ac.ir
Morteza Jalili Qazizadeh
m.jalili@qiet.ac.ir
Omid Movahedian
omidavazzadeh@gmail.com

¹ Department of Civil Engineering, Faculty of Engineering, Quchan University of Technology, P. O. Box. 94771-67335, Quchan, Iran

AFGM beams with power law and exponential law gradient. The Rayleigh–Ritz method and the finite element method were applied by Anandakumar and Kim, (2010) to study the modal behavior of a three-dimensional functionally graded (FG) cantilever beam. Ait Atmane et al., (2011) presented the analytical solutions for obtaining the natural frequencies of the exponential FGM beams with varying cross-section and classical boundary conditions.

The exact free vibration of the exponentially AFGM beams with different classical boundary conditions was performed by Li et al., (2013). Accordingly, they studied the effect of the exponential gradient index on the natural frequencies of the beam with various classical end supports. Çalloğlu et al., (2013) analyzed the free vibration of the symmetric FG sandwich beam with variable cross-section using the mixture rules and laminate theory. The free vibration of AFG non-uniform beams with different boundary conditions was studied by Rajasekaran, (2013) using the differential transformation-based dynamic stiffness approach. Duy et al., (2014) analyzed the free vibration of FGM beams on an elastic foundation and rotational spring supports. Tang et al., (2014) derived the exact frequency equations of the exponentially non-uniform AFG Timoshenko beam with different classical boundary conditions. The analytical solution was developed by Liu and Shu, (2014) to study the free vibration of the exponential FGM beams with single delamination. The exact natural frequencies of simply supported FGM beams with exponentially varying material properties were determined by Celebi and Tutuncu, (2014) using the plane elasticity theory. Kumar et al., (2015) investigated the nonlinear free vibration problem of AFG taper beams with the polynomial and exponential varying materials. Şimşek, (2015) analyzed the free and forced vibration behaviors of the bi-directional FGM Timoshenko beam with various boundary conditions. Ebrahimi and Mokhtari, (2015) investigated the vibration analysis of spinning exponentially FG Timoshenko beams based on the differential transform method.

The non-uniformity effects on the free vibration analysis of the non-uniform FGM beams with the exponential law and power law were discussed by Hosseini Hashemi et al., (2016). A novel method was proposed by Yuan et al., (2016) to obtain the exact solutions to the free vibrations of axially inhomogeneous and non-uniform Timoshenko beams. Wang et al., (2016) analyzed the free vibration of two-directional FGM beams with clamped-free and pinned–pinned end supports. By utilizing the displacement-based semi-analytical method, Lohar et al., (2016) presented the natural frequency and mode shapes of an exponential tapered AFG beam resting on an elastic foundation. Using the methods of initial parameters in differential form, the analysis of the free vibrations of the non-uniform and/or AFG Euler–Bernoulli beams with elastically restrained ends was performed by

Shvartsman and Majak, (2016). In that study, the power and exponential functions were utilized for variations of the geometrical and mechanical properties. The free transverse vibration analysis of AFG tapered Euler–Bernoulli beams through the spline finite point method was developed by Liu et al., (2016). They assumed the material types including power law and exponential law and discussed the natural frequencies of the beam with various classical boundary conditions. The analytical and numerical method for the free vibration of double-axially FGM beams with elastic end supports and exponential material properties were performed by Rezaiee-Pajand and Hozhabrossadati (2016a). Moreover, they studied the free vibration analysis of a double-beam system joined by a mass-spring device (Rezaiee-Pajand & Hozhabrossadati, 2016b).

The Chebyshev collocation method was applied by Wattanasakulpong and Mao, (2017) to study stability and vibration analyses of carbon nanotube-reinforced composite beams with elastic boundary conditions. By applying the Chebyshev polynomials, natural frequencies and mode shapes of tapered and AFG Rayleigh beams were examined by He et al., (2017). Using the Adomian decomposition method, the vibration analysis of the exponentially and trigonometrically tapered beams with nonlinearly axial varying FGM properties considering different geometry and material taper ratios was studied by Keshmiri et al., (2018). Karamanlı, (2018) analyzed the free vibration behavior of two-directional FGM beams subjected to various sets of classical boundary conditions by employing a third-order shear deformation theory. By a similar theory, the vibration analysis of FGM beams with elastic support was performed by Wattanasakulpong and Bui, (2018) using the Chebyshev collocation method. In another work, Wattanasakulpong et al., (2018) proposed the Chebyshev collocation approach for vibration analysis of FG porous beams based on third-order shear deformation theory.

The exact natural frequencies and buckling load of the FGM tapered beam-column with elastic supports were presented by Rezaiee-Pajand and Masoodi, (2018). Mahmoud, (2019) proposed a general solution for the free vibration of the non-uniform AFG cantilevers with tip mass at the free end using the transfer matrix method. Based on the new hybrid approach, the free vibration and stability analyses of AFGM Euler–Bernoulli beams with variable cross-sections resting on a uniform Winkler–Pasternak foundation were performed by Soltani and Asgarian, (2019). Avcar, (2019) investigated the free vibration of imperfect sigmoid and power law FG beams with simply supported. The analytical solution was presented by AlSaid-Alwan and Avcar, (2020) to study the free vibration of FG beams utilizing different types of beam theories. By using the Rayleigh–Ritz method, Kumar, (2020) investigated the dynamic behavior of an AFG beam resting on a variable elastic foundation. Erdurcan and

Cunedioğlu, (2020) studied the free vibration of an aluminum beam coated with FGM by using a Timoshenko beam and FEM theory for both simply supported and cantilever beams. The Chebyshev spectral collocation method was employed by Sari and Al-Dahidi, (2020) to study the vibration behavior of AFG non-uniform multiple beams. Avcar et al., (2021) analyzed the natural frequencies of sigmoid FG sandwich beams in the framework of high-order shear deformation theory. The continuous elements method was applied by Selmi, (2021) to investigate the free vibration bi-dimensional FGM beams. He considered that the material properties vary exponentially along the beam thickness and length. By a similar approach, Selmi and Mustafa, (2021) analyzed the influences of the gradient indexes and the beam slenderness ratio on the natural frequencies of the exponential BDFGM beams with simple supports. Chen and Chang, (2021) examined the vibration behaviors of BDFGM Timoshenko beams with classical boundary conditions, based on the Chebyshev collocation method. By a similar technique, the flexural vibration analysis of FG sandwich plates resting on an elastic foundation with arbitrary boundary conditions was performed by Tossapanon and Wattanasakulpong, (2020). Recently, the exact solutions for the free transverse vibration of power-law non-uniform AFG beams with endpoint masses and general boundary conditions were presented by Bambaeechee, (2022). Moreover, Zhao et al., (2022) proposed a unified Jacobi–Ritz approach for vibration analysis of FG porous rectangular plate with arbitrary boundary conditions based on a higher-order shear deformation theory.

A comprehensive literature review was completed above based on the focus on the works related to free vibration analysis of the FGM beams with the exponential variation of the material properties. To the best of the authors' knowledge, there is no reported work on the exact solutions of the free transverse vibration of the exponential AFGM beams with the concentrated tip masses and general boundary conditions. Thus, this study aims to get the closed-form expression for calculating the exact natural frequencies of the exponential AFGM Euler–Bernoulli beams with attached tip masses and general boundary conditions. In the following, the mode shapes and design charts of the AFGM beams can also be obtained. The advantages of the proposed formulations are high accuracy, generality, and simplicity to simulate the various boundary conditions. Also, it can be applied to the purposeful design of vibrating a wide range of uniform beams, non-uniform beams with constant thickness and exponentially decaying width, and composite beams. In addition, a similar strategy can be used for various material distribution. According to the derived formulations, the effects of the elastic supports, attached tip masses, and exponential gradient index on the natural frequencies and mode shapes of the exponential AFGM beams with symmetric and asymmetric boundary

conditions are investigated in detail for the first time. Results show they play an important role in the natural frequencies and mode shapes of the AFGM beams. This topic will be very important when the design goal is to achieve or not to achieve a certain frequency. Accordingly, the results of this study can be used for the proper design of the exponential composite beams carrying tip masses with different elastic boundary conditions. Moreover, the proposed method can be applied to study the behavior of the small-scale structures that are governed by the classical Euler–Bernoulli beam theory.

Free vibration analysis

In this work, the analytical solutions to obtain the exact natural frequencies of the exponential AFGM Euler–Bernoulli beam with general boundary conditions and attached tip masses are derived.

AFGM properties

In this study, the material properties, i.e., modulus of elasticity and mass density of the AFGM beam, shown in Fig. 1, are assumed to vary continuously and together in the axial direction according to the exponential functions and defined as (Li et al., 2013):

$$\rho(x) = \rho_0 e^{2\beta\left(\frac{x}{L}\right)} = \rho_L e^{2\beta\left(\frac{x}{L}-1\right)} \quad 0 \leq x \leq L \quad (1a)$$

$$E(x) = E_0 e^{2\beta\left(\frac{x}{L}\right)} = E_L e^{2\beta\left(\frac{x}{L}-1\right)} \quad 0 \leq x \leq L \quad (1b)$$

where β is the exponential gradient index, x is the axial coordinate, L is the length of the beam, $\rho(x)$ is the volume mass density at position x , and $E(x)$ is the modulus of elasticity at position x . Also, ρ_0 and E_0 , and ρ_L and E_L , are the mass density and modulus of elasticity at $x=0$ and $x=L$, respectively. Here, the subscript “0” means $x=0$, and the subscript “L” indicates $x=L$. As a result, the mass per unit length and flexural rigidity of the exponential AFGM was obtained as:

$$m(x) = \rho(x)A = \rho_0 A e^{2\beta\left(\frac{x}{L}\right)} = \rho_L A e^{2\beta\left(\frac{x}{L}-1\right)} \quad (2a)$$

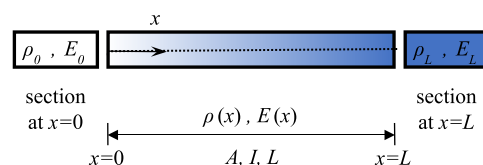


Fig. 1 Schematic of the exponential AFGM beam

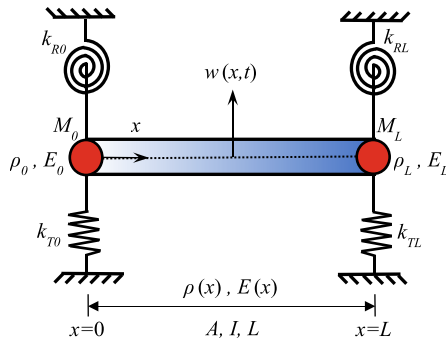


Fig. 2 Schematic of the exponential AFGM beam with general boundary conditions and tip masses

$$K(x) = E(x)I = E_0 I e^{2\beta(\frac{x}{L})} = E_L I e^{2\beta(\frac{x}{L}-1)} \tag{2b}$$

where $m(x)$, $K(x)$, A , and I are the mass per unit length, flexural rigidity, cross-section area, and moment of inertia of the AFGM beam, respectively. It should be noted that the exponential gradient index, β , can be any rational number. In addition, when $\beta=0$, the beam is homogeneous.

Governing differential equation

The free lateral vibration differential equation of an AFGM beam of length L with general boundary conditions and tip masses in the framework of the Euler–Bernoulli theory, as shown in Fig. 2, is given by (Rao, 2019):

$$\frac{\partial^2}{\partial x^2} \left[K(x) \frac{\partial^2 w(x, t)}{\partial x^2} \right] + m(x) \frac{\partial^2 w(x, t)}{\partial t^2} = 0, \quad 0 \leq x \leq L \tag{3}$$

where x is the axial coordinate, t is time, $w(x, t)$ is the lateral deflection of the beam, $K(x)$ is the flexural rigidity of the beam at the position x , and $m(x)$ is the mass per unit length of the beam at the position x .

Following the separation of variable analogy, the solution of Eq. (3) can be expressed as (Rao, 2019):

$$w_n(x, t) = W_n(x) \sin \omega_n t \tag{4}$$

where $W_n(x)$ is the shape function of the lateral motion of the n th vibration mode and ω_n is the circular frequency.

Substituting Eq. (4) into Eq. (3), one can get:

$$\frac{d^2}{dx^2} \left[K(x) \frac{d^2 W_n(x)}{dx^2} \right] - m(x) \omega_n^2 W_n(x) = 0 \tag{5}$$

If Eqs. (2a) and (2b) are inserted into Eq. (5), it can be rewritten as:

$$\frac{d^2}{dx^2} \left[E_0 I e^{2\beta(\frac{x}{L})} \frac{d^2 W_n(x)}{dx^2} \right] - \rho_0 A e^{2\beta(\frac{x}{L})} \omega_n^2 W_n(x) = 0 \tag{6}$$

By deriving from the latter equation, one can get:

$$E_0 I e^{2\beta(\frac{x}{L})} \frac{d^4 W_n(x)}{dx^4} + 4\beta \frac{E_0 I}{L} e^{2\beta(\frac{x}{L})} \frac{d^3 W_n(x)}{dx^3} + 4\beta^2 \frac{E_0 I}{L^2} e^{2\beta(\frac{x}{L})} \frac{d^2 W_n(x)}{dx^2} - \rho_0 A e^{2\beta(\frac{x}{L})} \omega_n^2 W_n(x) = 0 \tag{7}$$

or

$$L^4 \frac{d^4 W_n(x)}{dx^4} + 4\beta L^3 \frac{d^3 W_n(x)}{dx^3} + 4\beta^2 L^2 \frac{d^2 W_n(x)}{dx^2} - \omega_n^2 L^4 \frac{\rho_0 A}{E_0 I} W_n(x) = 0 \tag{8}$$

Introducing the following quantity

$$X = \frac{x}{L} \tag{9}$$

and considering in mind that

$$dx = L dX \tag{10}$$

Equation (8) simplifies as follows:

$$\frac{d^4 W_n(X)}{dX^4} + 4\beta \frac{d^3 W_n(X)}{dX^3} + 4\beta^2 \frac{d^2 W_n(X)}{dX^2} - \Omega_n^2 W_n(X) = 0 \tag{11}$$

where $\Omega_n = \omega_n L^2 \sqrt{\frac{\rho_0 A}{E_0 I}}$ is the dimensionless natural frequency coefficient of the n th vibration mode.

The general solution of this equation is (Wang & Wang, 2013):

$$W_n(X) = e^{-\beta X} [C_1 \cos(\delta_1 X) + C_2 \sin(\delta_1 X) + C_3 \cosh(\delta_2 X) + C_4 \sinh(\delta_2 X)] \quad \text{if } \Omega_n > \beta^2 \tag{12a}$$

$$W_n(X) = e^{-\beta X} [C_1 + C_2 X + C_3 \cosh(\delta_2 X) + C_4 \sinh(\delta_2 X)] \quad \text{if } \Omega_n = \beta^2 \tag{12b}$$

$$W_n(X) e^{-\beta X} [C_1 \cosh(\delta_3 X) + C_2 \sinh(\delta_3 X) + C_3 \cosh(\delta_2 X) + C_4 \sinh(\delta_2 X)] \quad \text{if } \Omega_n < \beta^2 \tag{12c}$$

where $\delta_1 = \sqrt{\Omega_n - \beta^2}$, $\delta_2 = \sqrt{\Omega_n + \beta^2}$, $\delta_3 = \sqrt{\beta^2 - \Omega_n}$, and C_1, C_2, C_3, C_4 are unknown constants. Although $\Omega_n > \beta^2$ in most cases, there are situations where $\Omega_n < \beta^2$ (Wang & Wang, 2013). Herein, just investigated the case $\Omega_n > \beta^2$ in detail which occurs in most cases.

General boundary conditions and tip masses

The boundary conditions of the exponential AFGM beam, in the presence of the concentrated tip masses M_0 and M_L , and constraints with the rotational elastic stiffnesses k_{R0} and k_{RL} , and lateral translational elastic stiffnesses k_{T0} and k_{TL} are expressed as:

$$\frac{d^2 W_n(X)}{dX^2} - \frac{k_{R0}L}{E_0I} \frac{dW_n(X)}{dX} = 0 \tag{13}$$

$$\frac{d^3 W_n(X)}{dX^3} + 2\beta \frac{d^2 W_n(X)}{dX^2} + \frac{(k_{T0} - M_0 \omega_n^2)L^3}{E_0I} W_n(X) = 0 \tag{14}$$

which refer to the equilibrium of bending and shear at $X=0$, respectively, and

$$\frac{d^2 W_n(X)}{dX^2} + \frac{k_{RL}L}{E_LI} \frac{dW_n(X)}{dX} = 0 \tag{15}$$

$$\frac{d^3 W_n(X)}{dX^3} + 2\beta \frac{d^2 W_n(X)}{dX^2} + \frac{(M_L \omega_n^2 - k_{TL})L^3}{E_LI} W_n(X) = 0 \tag{16}$$

which denote the equilibrium of bending and shear at $X=1$, respectively.

For simplicity, the following dimensionless mass ratios (α_0, α_L), stiffness coefficient (K_{R0}, K_{RL}, K_{T0} , and K_{TL}), and stiffness ratios (R_0, R_L, T_0 , and T_L) are introduced (Rezaiee-Pajand et al., 2015; Šalinić et al., 2018):

$$\alpha_0 = \frac{M_0}{\rho_0 AL}, \alpha_L = \frac{M_L}{\rho_L AL}, K_{R0} = \frac{k_{R0}L}{E_0I}, K_{T0} = \frac{k_{T0}L^3}{E_0I}, K_{RL} = \frac{k_{RL}L}{E_LI}, K_{TL} = \frac{k_{TL}L^3}{E_LI}, \tag{17}$$

$$R_0 = \frac{K_{R0}}{1 + K_{R0}}, T_0 = \frac{K_{T0}}{1 + K_{T0}}, R_L = \frac{K_{RL}}{1 + K_{RL}}, T_L = \frac{K_{TL}}{1 + K_{TL}}. \tag{23}$$

From above, the corresponding inverse relation between stiffness coefficients and stiffness ratios read:

$$K_{R0} = \frac{R_0}{1 - R_0}, K_{T0} = \frac{T_0}{1 - T_0}, K_{RL} = \frac{R_L}{1 - R_L}, K_{TL} = \frac{T_L}{1 - T_L}. \tag{18}$$

Accordingly, when the stiffness coefficients ($K_{R0}, K_{RL}, K_{T0}, K_{TL}$) vary from 0 to ∞ , the corresponding stiffness ratios (R_0, R_L, T_0 , and T_L) take values from 0 to 1. This makes

numerical calculations much easier because one avoids seeking the sufficiently large value of spring stiffness coefficients, which would adequately substitute value 1 in specific numerical calculations (Šalinić et al., 2018). As a result, if the stiffness ratios are allowed to become one or zero, then the classical restraints can be easily recovered. Also, the non-classical supports have stiffness ratios between zero and one. For example, the values $R_0 = T_0 = 1$ and $R_L = T_L = 0$ correspond to the clamped left and the free right end of the beam, respectively. The elastic beam whose stiffness of all elastic supports is 50%, is modeled by considering $R_0 = T_0 = R_L = T_L = 0.5$. Here, the subscript “0” denotes $x=0$, and the subscript “L” means $x=L$.

Substituting the values of X and dimensionless ratios defined as Eq. (17), the boundary conditions of Eqs. (13)–(16) can be expressed by the following dimensionless forms:

$$(1 - R_0)W_n''(0) - R_0W_n'(0) = 0 \tag{19}$$

$$(1 - T_0)W_n''''(0) + 2\beta(1 - T_0)W_n''(0) + [T_0 - \alpha_0\Omega_n^2(1 - T_0)]W_n(0) = 0 \tag{20}$$

$$(1 - R_L)W_n''(1) + R_LW_n'(1) = 0 \tag{21}$$

$$(1 - T_L)W_n''''(1) + 2\beta(1 - T_L)W_n''(1) + [\alpha_L\Omega_n^2(1 - T_L) - T_L]W_n(1) = 0 \tag{22}$$

where $W_n'(X) = \frac{dW_n(X)}{dX}$, $W_n''(X) = \frac{d^2W_n(X)}{dX^2}$, and $W_n''''(X) = \frac{d^4W_n(X)}{dX^4}$.

Determination of the natural frequency

By substituting the general solution (12a) into the dimensionless boundary conditions defined in Eqs. (19)–(22), for the four integration constants, a homogeneous system of four equations can be found as:

$$\begin{bmatrix} A_{11} & A_{12} & A_{13} & A_{14} \\ A_{21} & A_{22} & A_{23} & A_{24} \\ A_{31} & A_{32} & A_{33} & A_{34} \\ A_{41} & A_{42} & A_{43} & A_{44} \end{bmatrix} \begin{bmatrix} C_1 \\ C_2 \\ C_3 \\ C_4 \end{bmatrix} = \begin{bmatrix} 0 \\ 0 \\ 0 \\ 0 \end{bmatrix}$$

or in compact matrix form as follows:

$$AC = 0 \tag{24}$$

where the constant coefficients matrix \mathbf{A} for the exponential AFGM beams with any rational value of the gradient index is given explicitly in Appendix. To have a non-trivial solution, the determinant of this system must be zero:

$$\det \mathbf{A} = 0 \quad (25)$$

Consequently, the positive real roots of this equation are the natural frequencies of the AFGM beams with the tip masses and elastic end supports. It should be added, that these are calculated numerically and using the well-known numerical software MAPLE.

Verification and numerical examples

To demonstrate the accuracy and efficiency of the derived formulations, three numerical examples, shown in Fig. 3, are analyzed in this part. The results are compared with those obtained by other researchers in Tables 1, 2, and 3. From Tables 1, 2, and 3, it is observed that the proposed formulations for computing the natural frequencies have high accuracy and are easy to simulate the various classical and non-classical boundary conditions. Moreover, the formulation is applied for a wide range of uniform, non-uniform and composite beams.

Discussion and parametric studies

The effects of the attached tip masses, elastic supports, and exponential gradient index on the natural frequencies and mode shapes of the AFGM beams with classical and non-classical boundary conditions will be investigated in this section. Accordingly, the schematics of the case studies with non-classical boundary conditions illustrate in Fig. 4. Moreover, several design charts for the fundamental natural frequency of the AFGM beams with various boundary conditions will be presented, for the first time.

Effects of the classical boundary conditions with various exponential gradient index and tip mass

In this section, the effects of the exponential gradient index and tip mass at the free end on the natural frequency coefficients Ω_n ($n=1,2,3$) for beams with symmetric and asymmetric classical boundary conditions, namely, P–P, C–C, F–C, and C–F, are investigated. Here, C means clamped, P denotes pinned, and F indicates free. The numerical values of Ω_n ($n=1,2,3$) for these cases are tabulated in Table 4. It should be added that according to the same results, depending on the symmetric or asymmetric boundary conditions

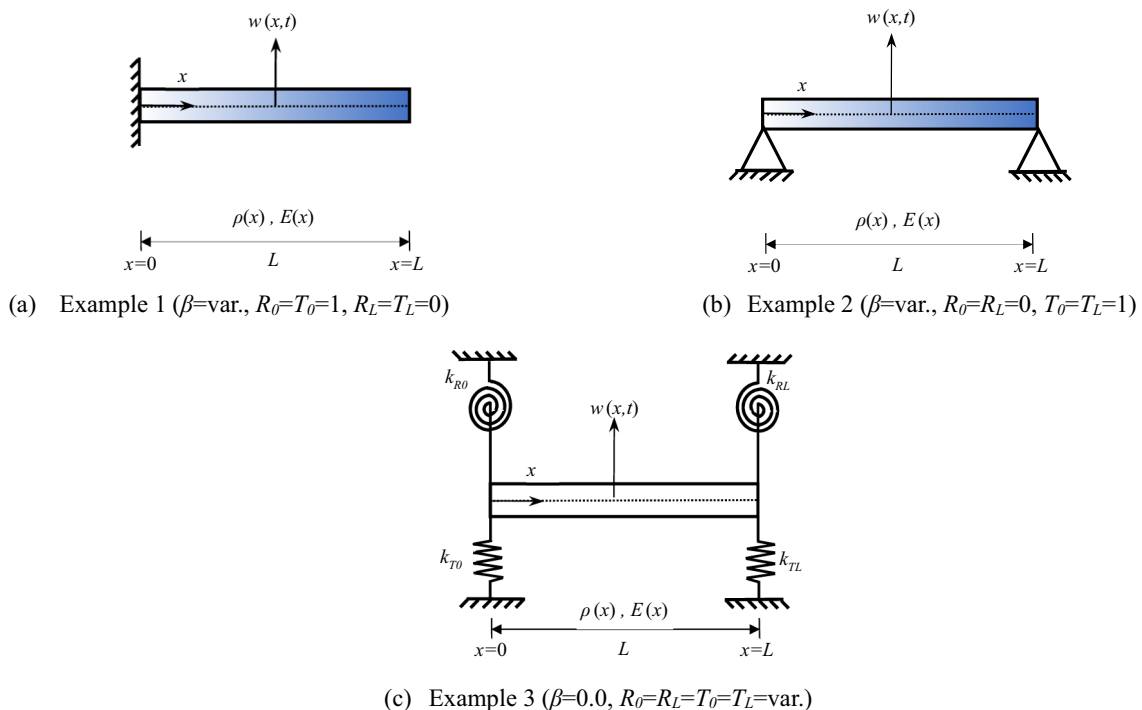


Fig. 3 Schematic of the exponential AFGM beams with classical boundary conditions and homogeneous beam with symmetric elastic boundary conditions in numerical examples

Table 1 The first three dimensionless natural frequencies of cantilever exponential AFGM beam for various β (Example 1)

β	Ω_n	Present	Selmi (2021)	Rezaiee-Pajand and Hozhabrossadati (2016a)	Wang et al., (2016)	Tang et al., (2014)	Çalloğlu et al., (2013)	Li et al., (2013)	Wang and Wang (2012)	Attarnejad et al., (2011)	Ait Amrane et al., (2011)
- 0.5	$n=1$	4.73491	4.7287	4.7350	4.735	4.73491	4.73491	4.73491	4.7349	4.7349	4.723
	$n=2$	24.20181	24.2015	24.2015	24.2018	24.20181	24.20181	24.20181	24.202	24.2018	24.2017
	$n=3$	63.86449	63.8643	63.8641	63.8645	63.86449	63.86449	63.86449	63.865	63.8645	63.8645
- 1.0	$n=1$	6.26264	-	6.2625	-	-	-	6.26264	6.2626	-	6.258
	$n=2$	26.58359	-	26.5833	-	-	-	26.58359	26.584	-	26.583
	$n=3$	66.37449	-	66.3752	-	-	-	66.3745	66.375	-	66.374

and the positive or negative sign of the exponential gradient index, this classification is considered.

From Table 4, it is deduced that the minimum and maximum of the natural frequency occur in the first mode of the uniform beam with C–C and P–P boundary conditions, respectively. Furthermore, for the C–C beam as the absolute value of β increases, the natural frequency coefficients increase. There is a similar situation for the P–P beam, except for the first natural frequency coefficient. On the other hand, as the exponential gradient index increases, the natural frequency coefficients of C–F and F–C beams increase and decrease, respectively. Accordingly, depending on the boundary conditions and mode of the vibration, changing the value of the exponential gradient index can cause a decrease or increase in the natural frequency of the exponential AFGM beam. For example, increasing the value of β from -1 to 1 can raise the fundamental natural frequency coefficient (Ω_1) of the F–C AFGM beam to 3.4 times. Although, this effect is lighter for the symmetric beam. Moreover, the natural frequencies of the exponential AFGM beam decrease with the increasing tip mass. Accordingly, the presence of tip mass as much as homogeneous beam mass at the free end can reduce the fundamental natural frequency coefficient (Ω_1) of the F–C beam by more than 50%, regardless of β .

Furthermore, Table 4 shows that two symmetric AFGM beams with symmetric exponential gradient indexes have the same natural frequency. On the other hand, two asymmetric AFGM beams with mirror boundary conditions and symmetric exponential gradient indexes have the same natural frequency. It is reminded that the uniform beams with C–F and F–C boundary conditions have the same natural frequencies but for the exponential AFGM beams, the corresponding results are different. The physical reasons for the differences in results for the exponential AFGM beams with C–F and F–C boundary conditions return to the equivalent lateral stiffness and tip mass. Accordingly, for the negative gradient index (corresponding to the trend of decreasing the flexural rigidity), the equivalent lateral stiffness of the C–F beam is larger than the F–C beam. Therefore, the natural frequencies of the C–F beam are larger than F–C beams with a negative gradient index. This phenomenon for the positive gradient index is inverted. In other words, for the positive gradient index (corresponding to the trend of increasing flexural rigidity), the equivalent lateral stiffness of the F–C beam is larger than the C–F beam. Therefore, the natural frequencies of the F–C beam are larger than C–F beams with a negative gradient index. However, the natural frequency decreases in the presence of tip mass, regardless of the boundary conditions.

Table 2 The first three dimensionless natural frequencies of simply supported exponential AFGM beam for various β (Example 2)

β	Ω_n	Present	Kumar (2020)	Soltani and Asgarian (2019)	He et al., (2017)	Hosseini Hashemi et al., (2016)	Li et al., (2013)	Ait Atmane et al., (2011)
0.5	$n=1$	9.77291	9.7731	9.7729	–	9.77300	–	9.773
	$n=2$	39.57036	39.5641	39.5704	–	39.56988	–	39.570
	$n=3$	88.97052	88.9004	88.9705	–	88.82628	–	88.970
1.0	$n=1$	9.48725	–	–	9.487253676	9.48689	9.48725	9.487
	$n=2$	39.85232	–	–	39.85231597	39.85245	39.85232	39.852
	$n=3$	89.40520	–	–	89.40520185	89.40458	89.40520	89.450

Table 3 The square root of the first three dimensionless natural frequencies of elastic supported homogeneous beam for various $R_0=R_L=T_0=T_L$ (Example 3)

β	$\sqrt{\Omega_n}$	$R_0=R_L=T_0=T_L$								
		1/2			5/6		10/11			
		Present	Bambaechee (2019)	Lai et al., (2008)	Present	Bambaechee (2019)	Present	Bambaechee (2019)	Lai et al., (2008)	
0.0	$n=1$	1.18564	1.1856	1.1856	1.76346	1.7635	2.08826	2.0883	2.0883	
	$n=2$	2.23331	2.2333	2.2333	2.97286	2.9729	3.27087	3.2709	3.2709	
	$n=3$	5.06314	5.0631	5.0631	5.63928	5.6393	5.90693	5.9069	5.9069	

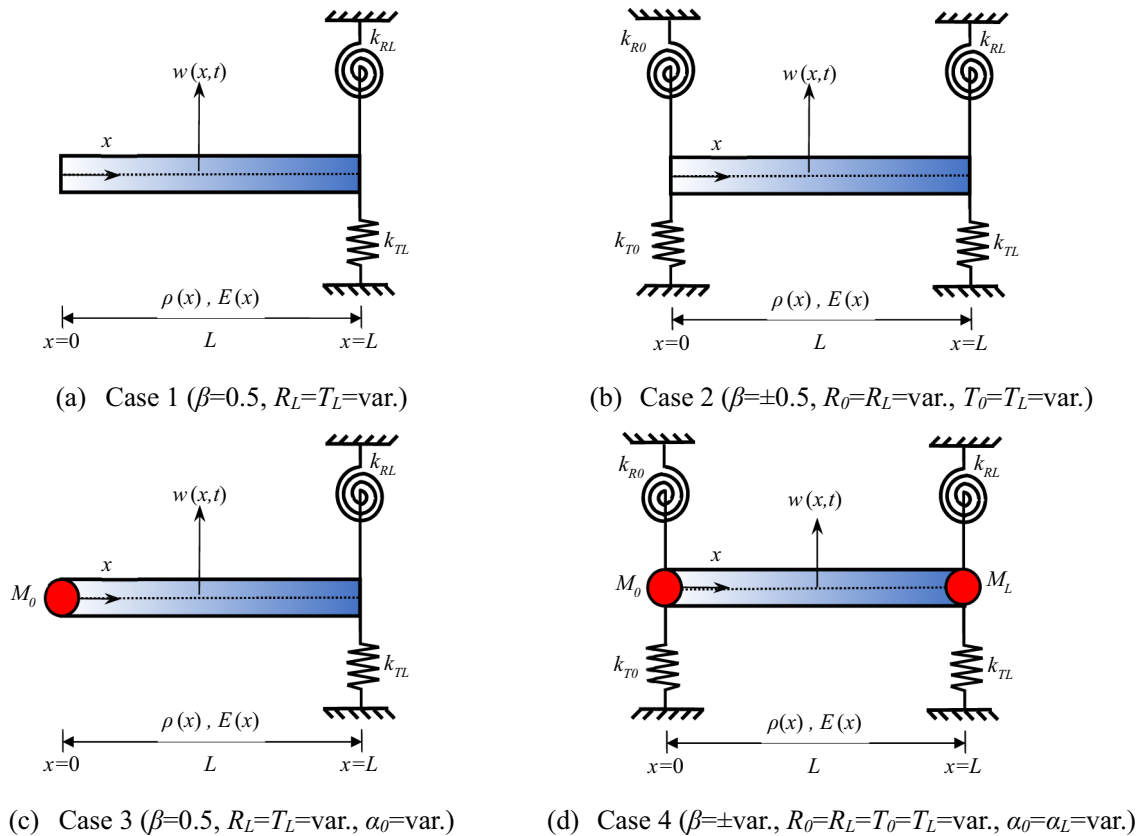


Fig. 4 Schematic of the exponential AFGM beams with non-classical boundary conditions in parametric studies

Table 4 The first three dimensionless natural frequency coefficients Ω_n , $n = 1, 2, 3$ of the exponential AFGM beams with classical supports and various values of β and tip mass

β	Ω_n	Symmetric boundary conditions		Asymmetric boundary conditions			
		P–P	C–C	F–C		C–F	
				$\alpha_0=0$	$\alpha_0=1$	$\alpha_L=0$	$\alpha_L=1$
– 1.0	$n=1$	9.4872	22.9377	1.8405	0.7274	6.2626	3.0888
	$n=2$	39.8523	62.4227	18.1721	13.8581	26.5835	18.9815
	$n=3$	89.4052	121.7227	58.3886	49.2366	66.3744	50.8958
– 0.5	$n=1$	9.7729	22.5116	2.5653	1.0733	4.7349	2.2167
	$n=2$	39.5703	61.8596	20.0383	15.0355	24.2018	17.5475
	$n=3$	88.9705	121.1079	59.8708	49.9211	63.8644	52.1586
0.0 (uniform)	$n=1$	9.8696	22.3732	3.5160	1.5573	3.5160	1.5573
	$n=2$	39.4784	61.6728	22.0344	16.2501	22.0344	16.2501
	$n=3$	88.8264	120.9033	61.6972	50.8958	61.6972	50.8958
0.5	$n=1$	9.7729	22.5116	4.7349	2.2167	2.5653	1.0733
	$n=2$	39.5703	61.8596	24.2018	17.5475	20.0383	15.0355
	$n=3$	88.9705	121.1079	63.8644	52.1586	59.8708	49.9211
1.0	$n=1$	9.4872	22.9377	6.2626	3.0888	1.8405	0.7274
	$n=2$	39.8523	62.4227	26.5835	18.9815	18.1721	13.8581
	$n=3$	89.4052	121.7227	66.3744	50.8958	58.3886	49.2366

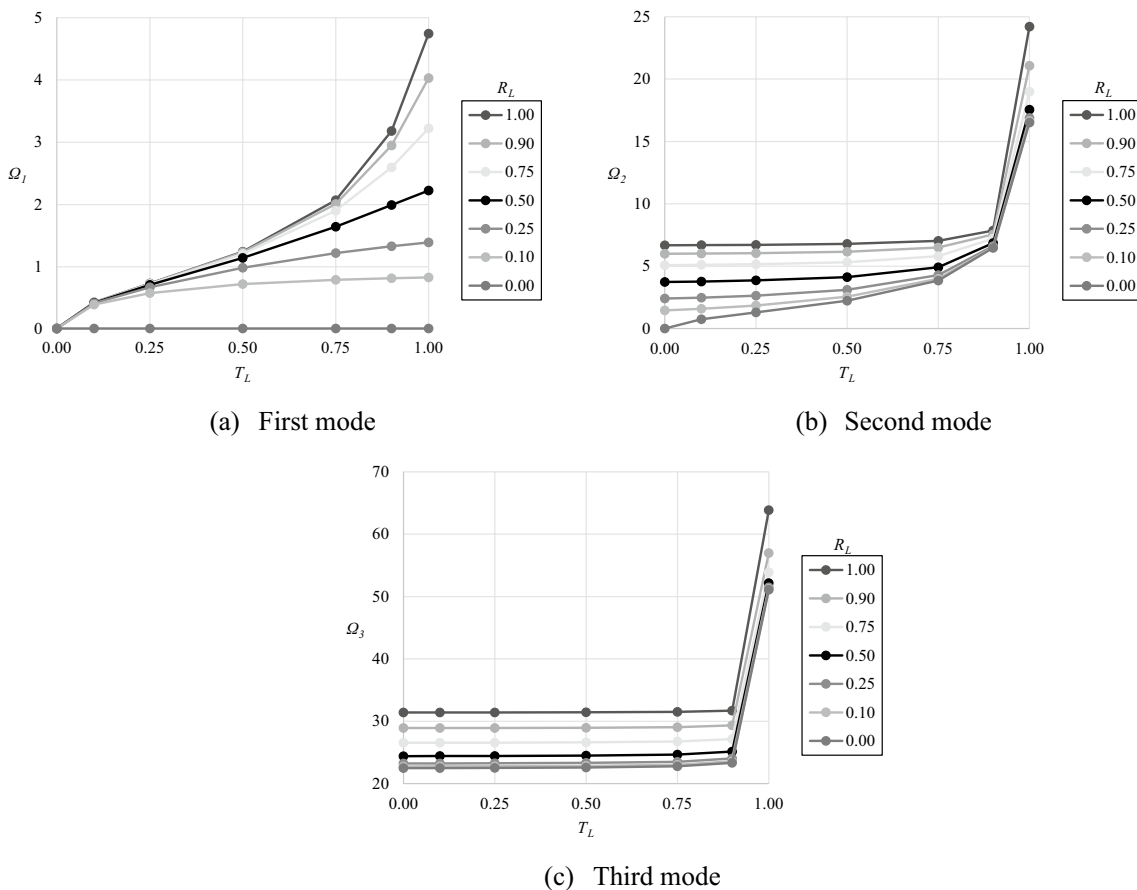


Fig. 5 Plot the first three dimensionless natural frequencies in case 1

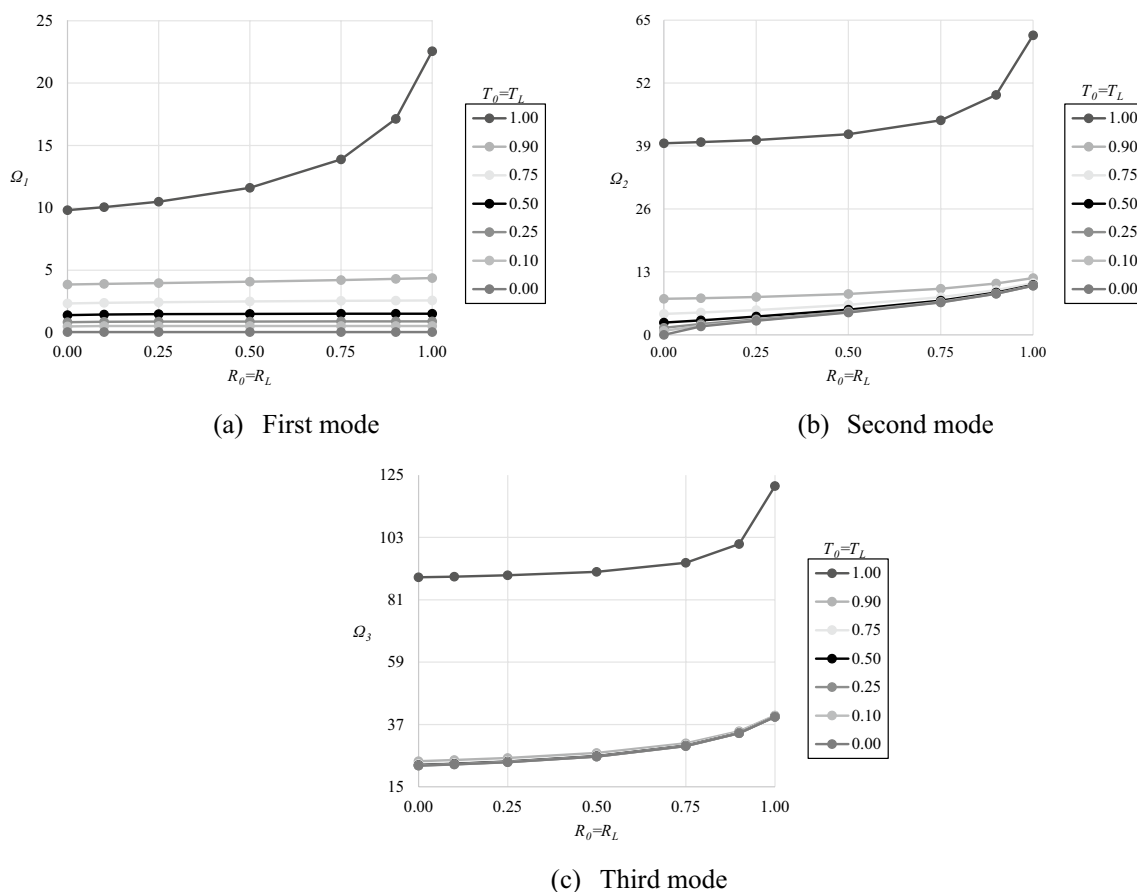


Fig. 6 Plot the first three dimensionless natural frequencies in case 2

Effects of the non-classical boundary conditions

In Figs. 5 and 6, variations of the first three dimensionless natural frequencies Ω_n ($n=1,2,3$) of the exponential AFGM beams ($\beta=0.5$) to various quantities of the rotational and translational stiffness ratios (i.e., T_0 , R_0 , T_L , and R_L) are plotted.

Asymmetric boundary conditions (Case 1)

In this case, the free-supported exponential AFGM beam ($\beta=0.5$) with the translational and rotational springs at $x=L$ (Fig. 4(a)) is studied. As seen in Fig. 5, as the stiffness ratios $R_L=T_L$ increase from 0 (corresponding to F–F beam) to 1 (corresponding to F–C beam), the natural frequencies of the AFGM beam increase. This effect is more pronounced as the rotational and translational stiffness ratios $R_L=T_L$ are more than 0.9. In other words, the translational stiffness sensitivity (slope of the T_L - Ω_n curve) is higher when the stiffness of the translational spring k_{TL} is more than 90%. Accordingly, increasing stiffnesses of the elastic support $R_L=T_L$ from 10 to 50% and 100% can increase the fundamental frequency

of the AFGM beam in case 1 by about 2.95 and 12.33 times, respectively.

Symmetric boundary conditions (Case 2)

In this case, the symmetric elastic supported exponential AFGM beam ($\beta=0.5$) with two translational and rotational springs at $x=0$ and $x=L$ (Fig. 4(b)) is investigated. According to Fig. 6, as the stiffness ratios $R_0=R_L=T_0=T_L$ increase from 0 (corresponding to the F–F beam) to 1 (corresponding to the C–C beam), the natural frequencies of the AFGM beam increase smoothly. Also, the value of Ω_1 is almost independent of the rotational stiffness, except in the limit state $T_0=T_L=1$ (corresponding to the P–P beam). It should be noted that when $T_0=T_L=1$, the trend of increasing frequencies is more intense and there is a significant difference between the values of Ω_n ($n=1,2,3$) with other states. Accordingly, increasing stiffnesses of the elastic support $R_0=R_L=T_0=T_L$ from 10 to 50% and 100% can raise the first dimensionless natural frequency coefficient Ω_1 of the AFGM beam in case 2 to 2.99 and 46.40 times, respectively.

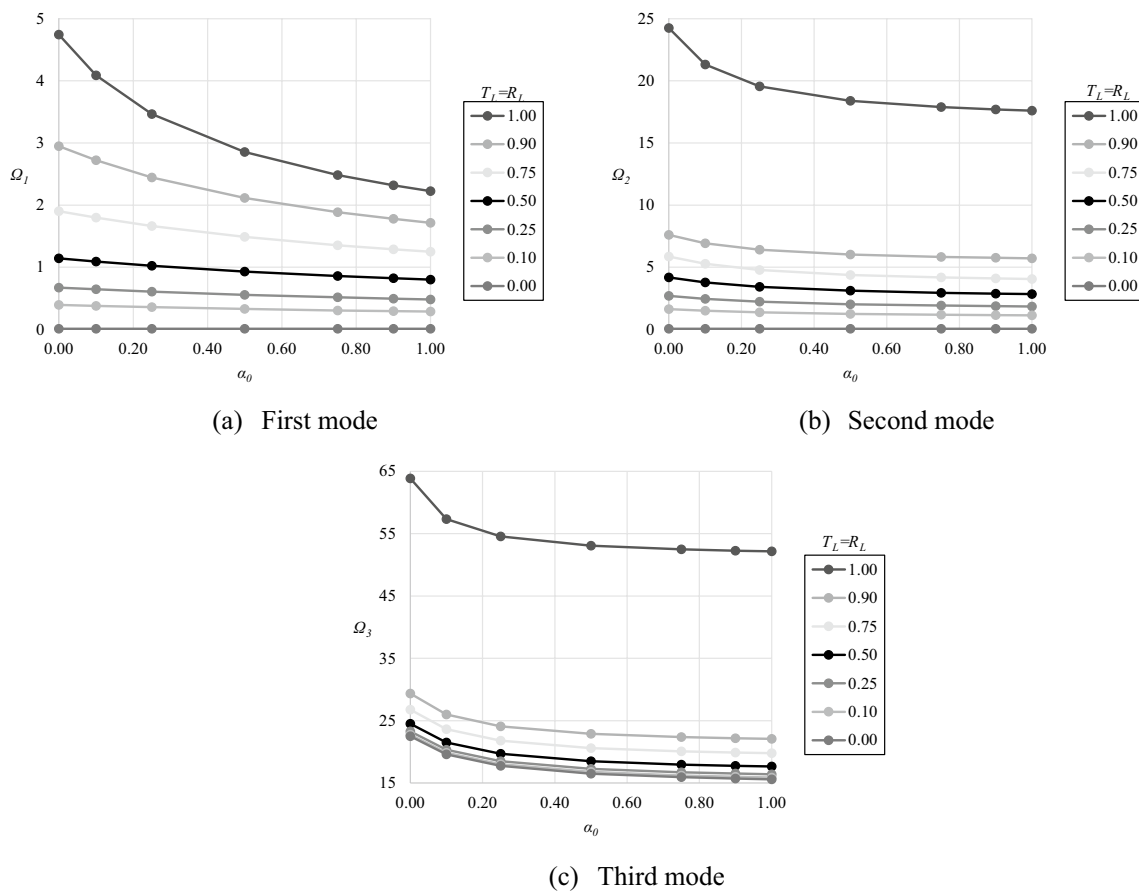


Fig. 7 Plot the first three dimensionless natural frequencies in case 3

Table 5 Sample results of the first three dimensionless natural frequencies for case 3

α_0	Ω_n	$R_L=T_L$		
		0.1 (low stiffness)	0.5 (moderate stiffness)	0.9 (high stiffness)
0.0	$n=1$	0.3840	1.1333	2.9390
	$n=2$	1.5873	4.1257	7.5564
	$n=3$	22.7788	24.4981	29.3623
0.5	$n=1$	0.3183	0.9216	2.1055
	$n=2$	1.1953	3.0597	5.9724
	$n=3$	16.7877	18.4992	22.8895
1.0	$n=1$	0.2762	0.7898	1.7061
	$n=2$	1.0854	2.7869	5.6729
	$n=3$	15.8931	17.6548	22.0763

From the comparison of Figs. 5 and 6, it is concluded that translational stiffness has relatively more influence on the natural frequencies than rotational stiffness.

Effects of the tip mass with asymmetric boundary conditions (Case 3)

Schematic of the third case study and variations of the first three dimensionless natural frequencies versus the mass ratio, α_0 , are plotted in Fig. 4(c) and Fig. 7, respectively. Furthermore, the sample results of the corresponding numerical values of Ω_n ($n=1,2,3$) for this case are listed in Table 5.

According to Fig. 7, increasing the tip mass ratio causes a reduction in the values of Ω_n ($n=1,2,3$) of the beam. This effect is more pronounced for the high stiffness and low tip mass ratios. From Fig. 7 and Table 5, it is observed that increasing the tip mass ratio from 0 to 1 can decrease the first dimensionless natural frequency coefficient Ω_1 of the AFGM beam for the low, moderate, high, and fully stiffness ratios in case 3 by about 28%, 30%, 42%, and 53%, respectively.

It is reminded that the result, in this case, can be used for the AFGM beam with $\beta=-0.5$ and mirror boundary conditions.

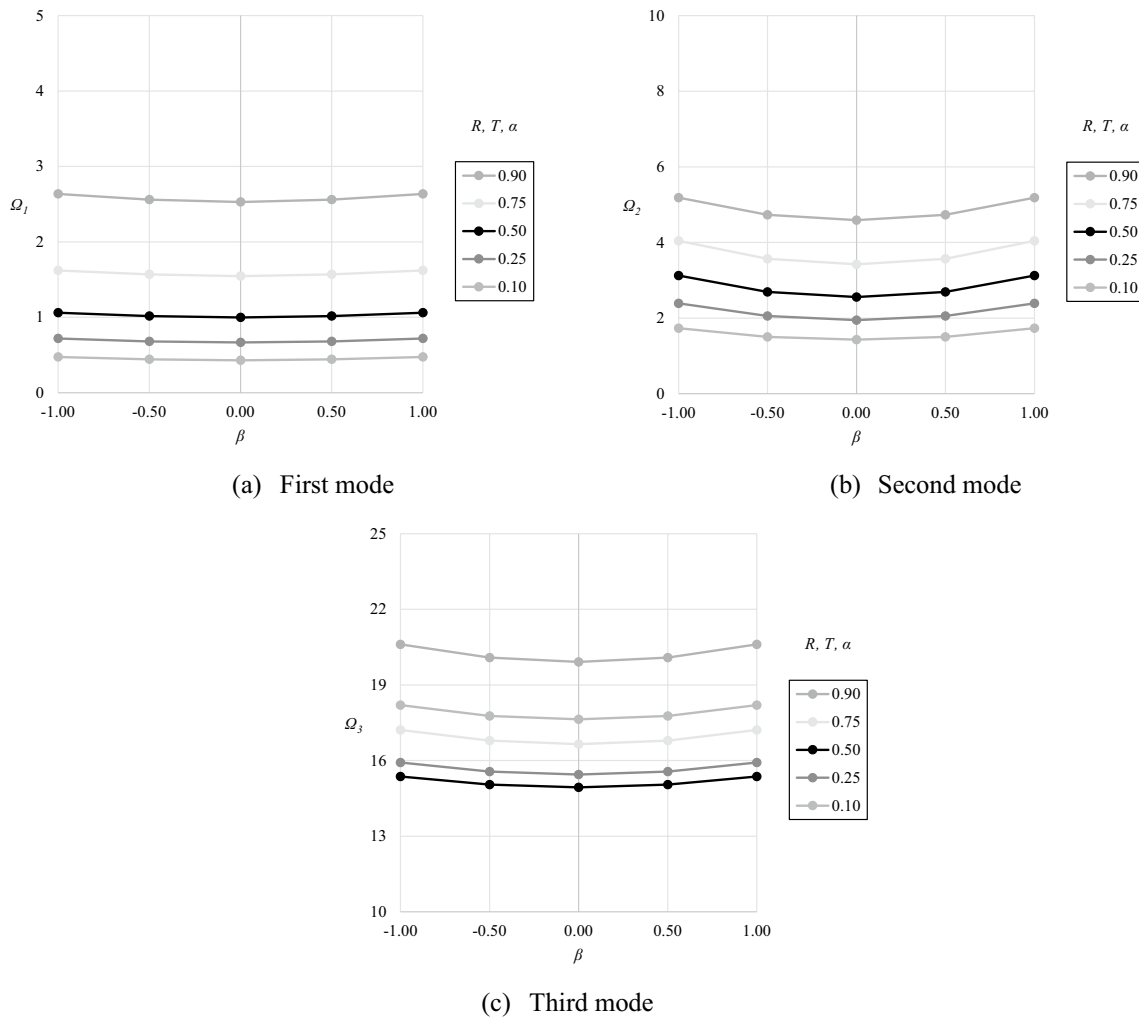


Fig. 8 Plot the first three dimensionless natural frequencies in case 4

Table 6 Sample results of the first three dimensionless natural frequencies for case 4

$ \beta $	Ω_n	$R_0=R_L=T_0=T_L=\alpha_0=\alpha_L$		
		0.1	0.5	0.9
0.0 (homogeneous)	$n=1$	0.4301	0.9985	2.5277
	$n=2$	1.4292	2.5580	4.5888
	$n=3$	17.6342	14.9381	19.9150
0.5	$n=1$	0.4414	1.0158	2.5590
	$n=2$	1.5046	2.6943	4.7302
	$n=3$	17.7722	15.0440	20.0868
1.0	$n=1$	0.4733*	1.0597	2.6364
	$n=2$	1.7337	3.1269	5.1829
	$n=3$	18.1986	15.3708	20.6069

Note: Values are from Eq. (12a) except for the value with asterisks, which is from Eq. (12c)

Effects of the exponential gradient index with symmetric boundary conditions (Case 4)

In Fig. 4(d) and Fig. 8, respectively, the schematic of the fourth case study and variations of the first three dimensionless natural frequencies versus the exponential gradient index, β , are presented. Moreover, the sample results of the corresponding numerical values of Ω_n ($n=1,2,3$) for this case are tabulated in Table 6.

According to Fig. 8 and Table 6, it is deduced that for the AFGM beam with the symmetric elastic boundary conditions and tip masses, the minimum natural frequency always occurs for the homogeneous beam. Also, the variation of the natural frequencies is symmetrical to the variation of the exponential gradient index when the boundary conditions are symmetrical.

Furthermore, it is found that the values of Ω_n ($n=1,2$) increase as the stiffness and mass ratios increase simultaneously, regardless of β . This trend for the third mode is

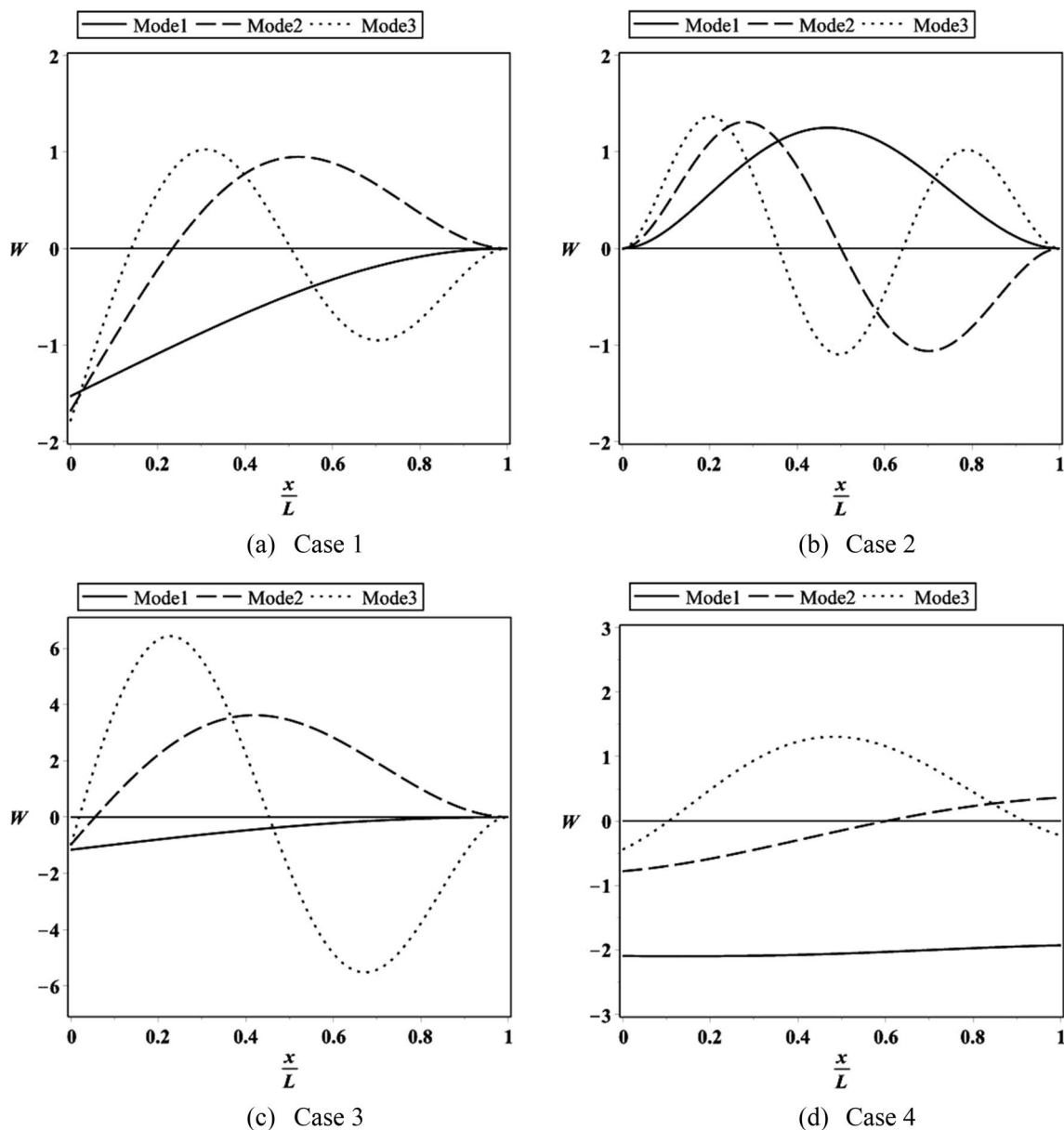


Fig. 9 Plot the first three mode shapes of the AFGM beam ($\beta=0.5$) in **a** case 1 with $R_L=T_L=1$, **b** case 2 with $R_0=T_0=R_L=T_L=1$, **c** case 3 with $R_L=T_L=1$ and $\alpha_0=1$, and **d** case 4 with $R_0=T_0=R_L=T_L=0.9$ and $\alpha_0=\alpha_L=0$

different and complex. Results show that for a homogeneous beam ($\beta=0$) and AFGM beam ($\beta=0.5$) with the simultaneous increase of each of the values of R_i , T_i , and α_i ($i=0, L$) from 0.1 to 0.9, the first natural frequency coefficient Ω_1 increases by about 5.88 and 5.80 times. Accordingly, the increasing effect of stiffness ratios is greater than the decreasing effect of tip mass ratios. On the other hand, increasing the exponential gradient index from 0 to 1 can increase the value of Ω_1 of the symmetric AFGM beam for the low, moderate, and high stiffness ratios by about 10%, 6%, and 4%, respectively.

Effects of the tip masses and various boundary conditions on the mode shapes

The first three mode shapes of the exponential AFGM beam ($\beta=0.5$) in cases 1 through 4 with various values of the variable parameters are plotted in Fig. 9. Those are obtained by solving the Eq. (23) by assuming $C_I=1$ and inserting it in Eq. (12a). Figure 9 illustrates that the tip mass (according to cases 1 and 3) and boundary conditions (according to cases 2 and 4) have a significant influence on the mode shapes of the AFGM beam, as expected. Also, the mode shapes of the

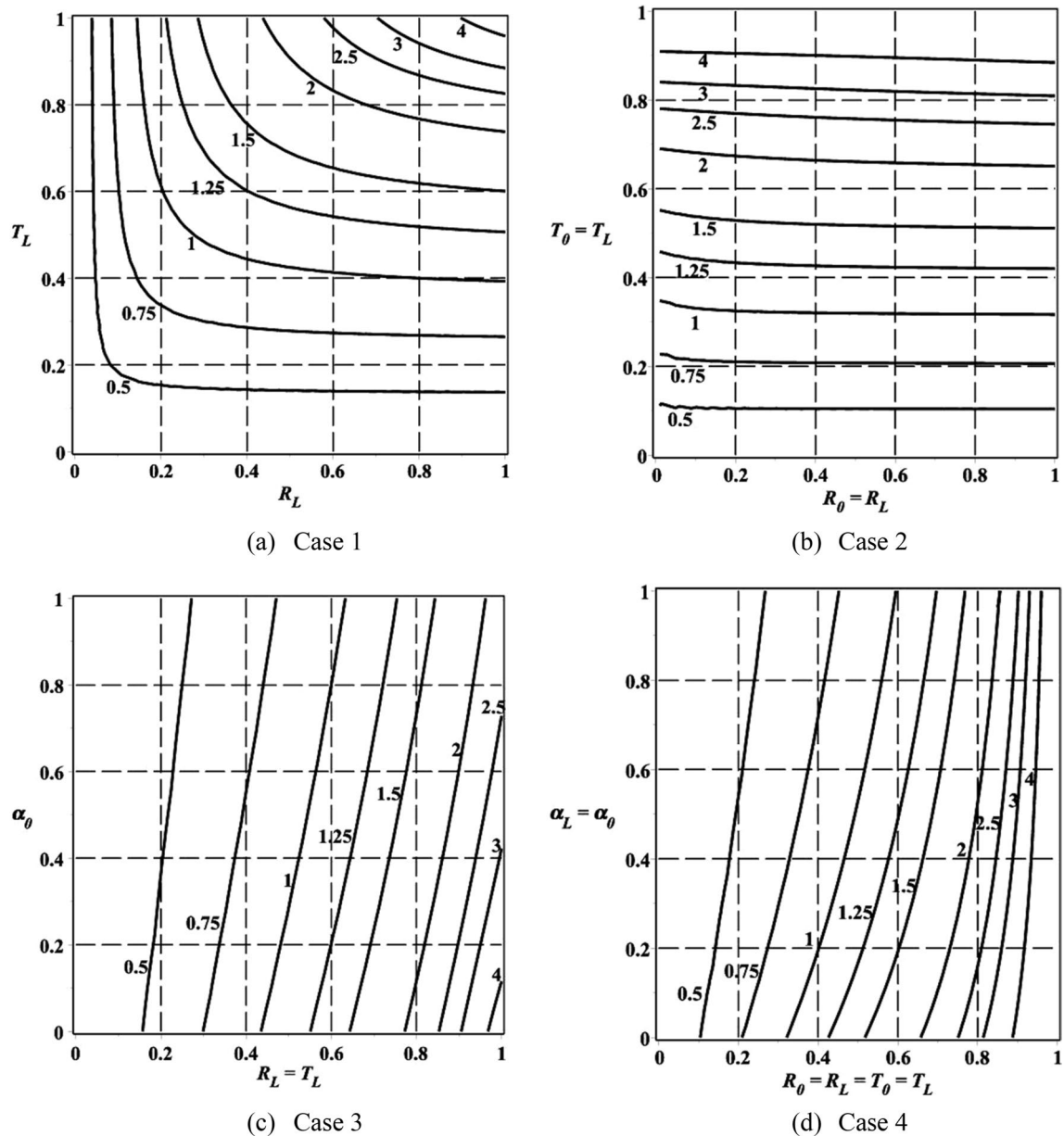


Fig. 10 Design charts for the fundamental dimensionless natural frequency (Ω_1) of the AFGM beam ($\beta=0.5$) with various boundary conditions

AFGM beam are always asymmetric because the material distribution is asymmetric.

Design charts for various boundary conditions

In this section, the design charts for the fundamental dimensionless natural frequency coefficient of the exponential AFGM beam ($\beta=0.5$) and homogenous beam ($\beta=0.0$) in the range $\Omega_1=0.5$ to $\Omega_1=4$ for cases 1 through 4 are illustrated in Fig. 10 and Fig. 11, respectively. Those are degenerated from the characteristic

equation (Eq. (25)) assuming a specific value of Ω_1 . From Figs. 10–11, in addition to confirmation of previous results, the possible combinations of the boundary conditions for specified fundamental natural frequencies are available. For example, the exponential AFGM beam ($\beta=0.5$) in case 1 with $R_L=0.2$ and $T_L=0.6$, or $R_L=0.8$ and $T_L=0.4$, case 2 with $T_0=T_L=0.35$, case 3 with $R_L=T_L=0.6$ and $\alpha_0=0.8$, and case 4 with $R_0=T_0=R_L=T_L=0.4$ and $\alpha_0=\alpha_L=0.2$ has the same fundamental natural frequency ($\Omega_1\approx 1$). Moreover, for known

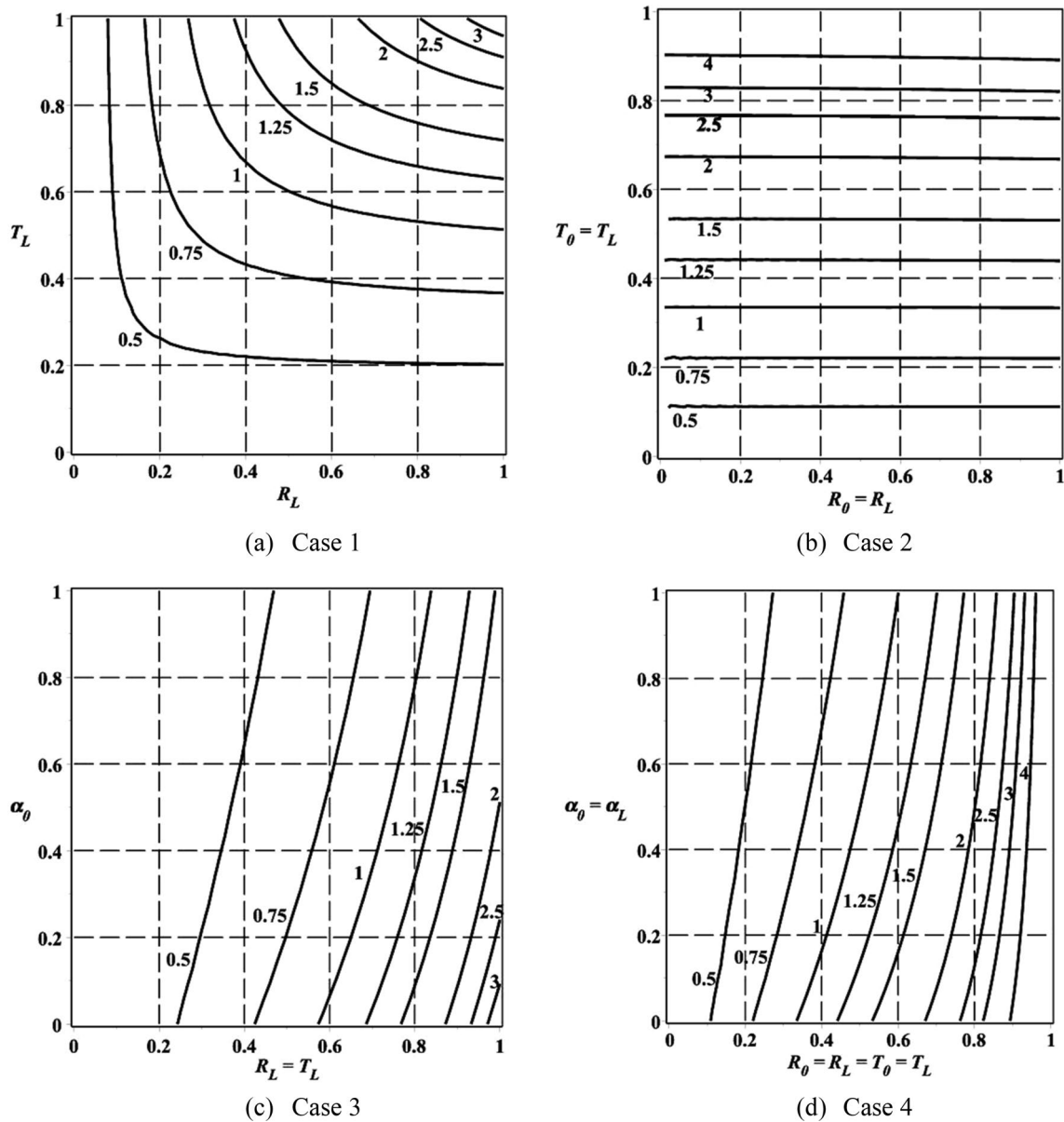


Fig. 11 Design charts for the fundamental dimensionless natural frequency (Ω_1) of the homogeneous beam ($\beta=0.0$) with various boundary conditions

boundary conditions, the design charts can be easily used to determine the value of Ω_1 .

By comparison of Fig. 10 and Fig. 11, it is concluded that the design charts of the homogeneous and inhomogeneous beams are very close to each other with symmetric boundary conditions. Nevertheless, there are the main differences between design charts of the homogeneous and inhomogeneous beams with asymmetric boundary conditions.

Conclusions

In this study, the analytical method and design charts for finding the exact solutions to the free transverse vibration of the AFGM beams with attached concentrated tip masses and general boundary conditions were presented in the framework of the Euler–Bernoulli theory. The material properties of AFGM beams were assumed to vary in the axial direction according to the exponential functions. The proposed formulations have high accuracy and efficiency and are usable for uniform, non-uniform, and composite beams. Moreover, a similar strategy could be used

for evaluating the other new variables in the free vibration analysis. According to the derived formulations, the effects of elastic supports, attached tip masses, and exponential gradient index on the natural frequencies and mode shapes of the exponential AFGM beams were discussed. Results show those play an important role in the natural frequencies and mode shapes of the AFGM beams. This topic would be very important when the design goal is to achieve or not to achieve a certain frequency. Accordingly, the results and design charts of this study could be used for the proper design of the exponential composite beams and homogeneous beams carrying tip masses with different elastic boundary conditions. Also, the exact solutions were reported in graphical and tabular forms and could be used as the benchmark for FEM and other numerical solutions.

Based on the parametric studies, the following important points are concluded:

- The natural frequencies of the AFGM beam decrease with the increasing tip mass ratio while increasing with increasing stiffness ratios. However, translational stiffness has relatively more influence than rotational stiffness.
- Depending on the boundary conditions and mode of the vibration, changing the value of the exponential gradient index β can cause a decrease or increase in the natural frequency of the exponential AFGM beam. Although, this effect is lighter for the symmetric beam.
- Asymmetric AFGM beams with mirror boundary conditions and mirror gradient index have the same natural frequency. For example, the natural frequencies of the free-clamped beam with exponential gradient index β are equal to the clamped-free beam with exponential gradient index $-\beta$.
- Symmetric AFGM beams for mirror gradient indexes have the same natural frequency. For example, the natural

frequencies of the pinned-pinned beam with exponential gradient index β and $-\beta$ are identical.

- The presence of tip mass as much as homogeneous beam mass at the free end of the free-clamped AFGM beam can reduce the fundamental natural frequency of the beam by more than 50%.
- For the symmetric AFGM beam with the non-classical boundary conditions, the minimum natural frequency occurs for the uniform beam. Nevertheless, for the simply supported AFGM beam, the maximum of the first natural frequency takes place in the homogeneous beam.

Appendix

The elements of the constant coefficients matrix, **A** for the exponential AFGM beam with carrying tip masses and various elastic boundary conditions in the framework of the Euler–Bernoulli theory are as follows:

$$A_{11} = (\delta_1^2 - \beta^2)(1 - R_0) - R_0\beta \tag{A-1}$$

$$A_{12} = \delta_1 [2\beta(1 - R_0) + R_0] \tag{A-2}$$

$$A_{13} = -(\delta_2^2 + \beta^2)(1 - R_0) - R_0\beta \tag{A-3}$$

$$A_{14} = \delta_2 [2\beta(1 - R_0) + R_0] \tag{A-4}$$

$$A_{21} = [-\beta(\delta_1^2 + \beta^2) + \Omega^2\alpha_0](1 - T_0) - T_0 \tag{A-5}$$

$$A_{22} = \delta_1 (\delta_1^2 + \beta^2)(1 - T_0) \tag{A-6}$$

$$A_{23} = [\beta(\delta_1^2 - \beta^2) + \Omega^2\alpha_0](1 - T_0) - T_0 \tag{A-7}$$

$$A_{24} = \delta_2 (\beta^2 - \delta_1^2)(1 - T_0) \tag{A-8}$$

$$A_{31} = e^{-\beta} \{ [(\delta_1^2 - \beta^2) \cos(\delta_1) - 2\beta\delta_1 \sin(\delta_1)] (1 - R_L) + (\beta \cos(\delta_1) + \delta_1 \sin(\delta_1))R_L \} \tag{A-9}$$

$$A_{32} = e^{-\beta} \{ [(\delta_1^2 - \beta^2) \sin(\delta_1) + 2\beta\delta_1 \cos(\delta_1)] (1 - R_L) + (\beta \sin(\delta_1) - \delta_1 \cos(\delta_1))R_L \} \tag{A-10}$$

$$A_{33} = e^{-\beta} \{ [-(\delta_2^2 + \beta^2) \cosh(\delta_2) + 2\beta\delta_2 \sinh(\delta_2)] (1 - R_L) + (\beta \cosh(\delta_2) - \delta_2 \sinh(\delta_2))R_L \} \tag{A-11}$$

$$A_{34} = e^{-\beta} \{ [-(\delta_2^2 + \beta^2) \sinh(\delta_2) + 2\beta\delta_2 \cosh(\delta_2)] (1 - R_L) + (\beta \sinh(\delta_2) - \delta_2 \cosh(\delta_2))R_L \} \tag{A-12}$$

$$A_{41} = e^{-\beta} \{ [(\delta_1^2 + \beta^2)(\delta_1 \sin(\delta_1) + \beta \cos(\delta_1)) + \Omega^2 \alpha_L \cos(\delta_1)] (1 - T_L) - \cos(\delta_1) T_L \} \quad (\text{A-13})$$

$$A_{42} = e^{-\beta} \{ [(\delta_1^2 + \beta^2)(\delta_1 \cos(\delta_1) - \beta \sin(\delta_1)) - \Omega^2 \alpha_L \sin(\delta_1)] (1 - T_L) + \sin(\delta_1) T_L \} \quad (\text{A-14})$$

$$A_{43} = e^{-\beta} \{ [(\delta_2^2 - \beta^2)(\beta \cosh(\delta_2) - \delta_2 \sinh(\delta_2)) - \Omega^2 \alpha_L \cosh(\delta_2)] (1 - T_L) + \cosh(\delta_2) T_L \} \quad (\text{A-15})$$

$$A_{44} = e^{-\beta} \{ [(\delta_2^2 - \beta^2)(\beta \sinh(\delta_2) - \delta_2 \cosh(\delta_2)) - \Omega^2 \alpha_L \sinh(\delta_2)] (1 - T_L) + \sinh(\delta_2) T_L \} \quad (\text{A-16})$$

Author contributions Bambaeechee Mohsen: Conceptualization, Methodology, Software, Formal analysis, Investigation, Writing-Original draft preparation, Writing- Reviewing and Editing, Visualization Supervision. Qazizadeh Morteza Jalili: Investigation, Resources, Writing- Reviewing and Editing. Movahedian Omid: Software, Formal analysis, Validation, Investigation, Reviewing.

Funding The authors received no financial support for the research, authorship, and/or publication of this article.

Declarations

Competing interests The authors declare no competing interests.

Conflict of interests The authors declared no potential conflicts of interest with respect to the research, authorship, and/or publication of this article.

References

- Ait Atmane, H., Tounsi, A., Meftah, S. A., & Belhadj, H. A. (2011). Free vibration behavior of exponential functionally graded beams with varying cross-section. *Journal of Vibration and Control*, 17(2), 311–318. <https://doi.org/10.1177/1077546310370691>
- AlSaid-Alwan, H. H. S., & Avcar, M. (2020). Analytical solution of free vibration of FG beam utilizing different types of beam theories: A comparative study. *Computers and Concrete*, 26(3), 285–292. <https://doi.org/10.12989/cac.2020.26.3.285>
- Anandakumar, G., & Kim, J.-H. (2010). On the modal behavior of a three-dimensional functionally graded cantilever beam: Poisson's ratio and material sampling effects. *Composite Structures*, 92(6), 1358–1371. <https://doi.org/10.1016/j.compstruct.2009.11.020>
- Attarnejad, R., Shahba, A., & Eslaminia, M. (2011). Dynamic basic displacement functions for free vibration analysis of tapered beams. *Journal of Vibration and Control*, 17(14), 2222–2238. <https://doi.org/10.1177/1077546310396430>
- Avcar, M. (2019). Free vibration of imperfect sigmoid and power law functionally graded beams. *Steel and Composite Structures*, 30(6), 603–615. <https://doi.org/10.12989/scs.2019.30.6.603>
- Avcar, M., Hadji, L., & Civalek, Ö. (2021). Natural frequency analysis of sigmoid functionally graded sandwich beams in the framework of high order shear deformation theory. *Composite Structures*, 276, 114564. <https://doi.org/10.1016/j.compstruct.2021.114564>
- Bambaeechee, M. (2019). Free vibration of AFG beams with elastic end restraints. *Steel and Composite Structures*, 33(3), 403–432. <https://doi.org/10.12989/scs.2019.33.3.403>
- Bambaeechee, M. (2022). Free transverse vibration of general power-law NAFG beams with tip masses. *Journal of Vibration Engineering & Technologies*. <https://doi.org/10.1007/s42417-022-00519-7>
- Çallioğlu, H., Demir, E., Yılmaz, Y., & Sayer, M. (2013). Vibration analysis of functionally graded sandwich beam with variable cross-section. *Mathematical and Computational Applications*, 18(3), 351–360. <https://doi.org/10.3390/mca18030351>
- Celebi, K., & Tutuncu, N. (2014). Free vibration analysis of functionally graded beams using an exact plane elasticity approach. *Proceedings of the Institution of Mechanical Engineers, Part c: Journal of Mechanical Engineering Science*, 228(14), 2488–2494. <https://doi.org/10.1177/0954406213519974>
- Chen, W.-R., & Chang, H. (2021). Vibration analysis of bidirectional functionally graded Timoshenko beams using Chebyshev collocation method. *International Journal of Structural Stability and Dynamics*, 21(01), 2150009. <https://doi.org/10.1142/S0219455421500097>
- Duy, H. T., Van, T. N., & Noh, H. C. (2014). Eigen analysis of functionally graded beams with variable cross-section resting on elastic supports and elastic foundation. *Structural Engineering and Mechanics*, 52(5), 1033–1049. <https://doi.org/10.12989/sem.2014.52.5.1033>
- Ebrahimi, F., & Mokhtari, M. (2015). Vibration analysis of spinning exponentially functionally graded Timoshenko beams based on differential transform method. *Proceedings of the Institution of Mechanical Engineers, Part g: Journal of Aerospace Engineering*, 229(14), 2559–2571. <https://doi.org/10.1177/0954410015580801>
- Erdurcan, E. F., & Cunedioğlu, Y. (2020). Free vibration analysis of a functionally graded material coated aluminum beam. *AIAA Journal*, 58(2), 949–954. <https://doi.org/10.2514/1.J059002>
- He, M.-F., Huang, Y., & Rong, H.-W. (2017). An efficient approach for the calculation of eigenfrequencies and mode shapes of tapered and axially functionally graded Rayleigh beams. *Acta Acustica United with Acustica*, 103(2), 276–287. <https://doi.org/10.3813/AAA.919056>
- Hosseini Hashemi, S., Bakhshi Khaniki, H., & Bakhshi Khaniki, H. (2016). Free vibration analysis of functionally graded materials non-uniform beams. *International Journal of Engineering - Transactions c: Aspects*, 29(12), 1734–1740. <https://doi.org/10.5829/idosi.ije.2016.29.12c.12>
- Huang, Y., & Li, X.-F. (2010). A new approach for free vibration of axially functionally graded beams with non-uniform cross-section. *Journal of Sound and Vibration*, 329(11), 2291–2303. <https://doi.org/10.1016/j.jsv.2009.12.029>
- Karamanlı, A. (2018). Free vibration analysis of two directional functionally graded beams using a third order shear deformation

- theory. *Composite Structures*, 189, 127–136. <https://doi.org/10.1016/j.compstruct.2018.01.060>
- Keshmiri, A., Wu, N., & Wang, Q. (2018). Vibration analysis of non-uniform tapered beams with nonlinear FGM properties. *Journal of Mechanical Science and Technology*, 32(11), 5325–5337. <https://doi.org/10.1007/s12206-018-1031-x>
- Kumar, S. (2020). Dynamic behaviour of axially functionally graded beam resting on variable elastic foundation. *Archive of Mechanical Engineering*, 67(4), 451–470. <https://doi.org/10.24425/ame.2020.131700>
- Kumar, S., Mitra, A., & Roy, H. (2015). Geometrically nonlinear free vibration analysis of axially functionally graded taper beams. *Engineering Science and Technology, an International Journal*, 18(4), 579–593. <https://doi.org/10.1016/j.jestch.2015.04.003>
- Lai, H.-Y., Hsu, J.-C., & Chen, C.-K. (2008). An innovative eigenvalue problem solver for free vibration of Euler-Bernoulli beam by using the Adomian decomposition method. *Computers & Mathematics with Applications*, 56(12), 3204–3220. <https://doi.org/10.1016/j.camwa.2008.07.029>
- Li, X.-F., Kang, Y.-A., & Wu, J.-X. (2013). Exact frequency equations of free vibration of exponentially functionally graded beams. *Applied Acoustics*, 74(3), 413–420. <https://doi.org/10.1016/j.apacoust.2012.08.003>
- Liu, P., Lin, K., Liu, H., & Qin, R. (2016). Free transverse vibration analysis of axially functionally graded tapered Euler-Bernoulli beams through spline finite point method. *Shock and Vibration*, 2016, 5891030-1–5891123. <https://doi.org/10.1155/2016/5891030>
- Liu, Y., & Shu, D. W. (2014). Free vibration analysis of exponential functionally graded beams with a single delamination. *Composites Part b: Engineering*, 59, 166–172. <https://doi.org/10.1016/j.compositesb.2013.10.026>
- Lohar, H., Mitra, A., & Sahoo, S. (2016). Natural frequency and mode shapes of exponential tapered AFG beams on elastic foundation. *International Frontier Science Letters*, 9, 9–25. <https://doi.org/10.18052/www.scipress.com/IFSL.9.9>
- Mahmoud, M. A. (2019). Natural frequency of axially functionally graded, tapered cantilever beams with tip masses. *Engineering Structures*, 187, 34–42. <https://doi.org/10.1016/j.engstruct.2019.02.043>
- Rajasekaran, S. (2013). Buckling and vibration of axially functionally graded nonuniform beams using differential transformation based dynamic stiffness approach. *Meccanica*, 48(5), 1053–1070. <https://doi.org/10.1007/s11012-012-9651-1>
- Rao, S. S. (2019). *Vibration of Continuous Systems* (2nd Edition). New York: John Wiley & Sons Inc. <https://doi.org/10.1002/9781119424284>
- Rezaiee-Pajand, M., & Hozhabrossadati, S. M. (2016a). Analytical and numerical method for free vibration of double-axially functionally graded beams. *Composite Structures*, 152, 488–498. <https://doi.org/10.1016/j.compstruct.2016.05.003>
- Rezaiee-Pajand, M., & Hozhabrossadati, S. M. (2016b). Free vibration analysis of a double-beam system joined by a mass-spring device. *Journal of Vibration and Control*, 22(13), 3004–3017. <https://doi.org/10.1177/1077546314557853>
- Rezaiee-Pajand, M., & Masoodi, A. R. (2018). Exact natural frequencies and buckling load of functionally graded material tapered beam-columns considering semi-rigid connections. *Journal of Vibration and Control*, 24(9), 1787–1808. <https://doi.org/10.1177/1077546316668932>
- Rezaiee-Pajand, M., Shahabian, F., & Bambaeechee, M. (2015). Buckling analysis of semi-rigid gabled frames. *Structural Engineering and Mechanics*, 55(3), 605–638. <https://doi.org/10.12989/sem.2015.55.3.605>
- Šalinić, S., Obradović, A., & Tomović, A. (2018). Free vibration analysis of axially functionally graded tapered, stepped, and continuously segmented rods and beams. *Composites Part b: Engineering*, 150, 135–143. <https://doi.org/10.1016/j.compositesb.2018.05.060>
- Sari, M. S., & Al-Dahidi, S. (2020). Vibration characteristics of multiple functionally graded nonuniform beams. *Journal of Vibration and Control*. <https://doi.org/10.1177/1077546320956768>
- Selmi, A., & Mustafa, A. A. (2021). Dynamic analysis of bi-dimensional functionally graded beams. *Materials Today: Proceedings*. <https://doi.org/10.1016/j.matpr.2021.03.726>
- Selmi, A. (2021). Vibration behavior of bi-dimensional functionally graded beams. *Structural Engineering and Mechanics*, 77(5), 587–599. <https://doi.org/10.12989/sem.2021.77.5.587>
- Shvartsman, B. S., & Majak, J. (2016). Free vibration analysis of axially functionally graded beams using method of initial parameters in differential form. *Advances in Theoretical and Applied Mechanics*, 9, 31–42. <https://doi.org/10.12988/atam.2016.635>
- Şimşek, M. (2015). Bi-directional functionally graded materials (BDFGMs) for free and forced vibration of Timoshenko beams with various boundary conditions. *Composite Structures*, 133, 968–978. <https://doi.org/10.1016/j.compstruct.2015.08.021>
- Soltani, M., & Asgarian, B. (2019). New hybrid approach for free vibration and stability analyses of axially functionally graded Euler-Bernoulli beams with variable cross-section resting on uniform Winkler-Pasternak foundation. *Latin American Journal of Solids and Structures*, 16(3), 173-1–173-25. <https://doi.org/10.1590/1679-78254665>
- Tang, A.-Y., Wu, J.-X., Li, X.-F., & Lee, K. Y. (2014). Exact frequency equations of free vibration of exponentially non-uniform functionally graded Timoshenko beams. *International Journal of Mechanical Sciences*, 89(Supplement C), 1–11. <https://doi.org/10.1016/j.ijmecsci.2014.08.017>
- Tossapanon, P., & Wattanasakulpong, N. (2020). Flexural vibration analysis of functionally graded sandwich plates resting on elastic foundation with arbitrary boundary conditions: Chebyshev collocation technique. *Journal of Sandwich Structures & Materials*, 22(2), 156–189. <https://doi.org/10.1177/1099636217736003>
- Wang, C. Y., & Wang, C. M. (2012). Exact vibration solution for exponentially tapered cantilever with tip mass. *Journal of Vibration and Acoustics*, 134(4), 041012-1–041012-4. <https://doi.org/10.1115/1.4005835>
- Wang, C. Y., & Wang, C. M. (2013). *Structural Vibration: Exact Solutions for Strings, Membranes, Beams, and Plates* (1 edition). Boca Raton, Florida: CRC Press. <https://doi.org/10.1201/b15348>
- Wang, Z., Wang, X., Xu, G., Cheng, S., & Zeng, T. (2016). Free vibration of two-directional functionally graded beams. *Composite Structures*, 135, 191–198. <https://doi.org/10.1016/j.compstruct.2015.09.013>
- Wattanasakulpong, N., & Bui, T. Q. (2018). Vibration analysis of third-order shear deformable FGM beams with elastic support by Chebyshev collocation method. *International Journal of Structural Stability and Dynamics*, 18(05), 1850071. <https://doi.org/10.1142/S0219455418500712>
- Wattanasakulpong, N., Chaikittiratana, A., & Pornpeerakeat, S. (2018). Chebyshev collocation approach for vibration analysis of functionally graded porous beams based on third-order shear deformation theory. *Acta Mechanica Sinica*, 34(6), 1124–1135. <https://doi.org/10.1007/s10409-018-0770-3>
- Wattanasakulpong, N., & Mao, Q. (2017). Stability and vibration analyses of carbon nanotube-reinforced composite beams with elastic boundary conditions: Chebyshev collocation method. *Mechanics of Advanced Materials and Structures*, 24(3), 260–270. <https://doi.org/10.1080/15376494.2016.1142020>
- Yuan, J., Pao, Y.-H., & Chen, W. (2016). Exact solutions for free vibrations of axially inhomogeneous Timoshenko beams with variable

cross section. *Acta Mechanica*, 227(9), 2625–2643. <https://doi.org/10.1007/s00707-016-1658-6>

Zhao, Y., Qin, B., Wang, Q., & Liang, X. (2022). A unified Jacobi-Ritz approach for vibration analysis of functionally graded porous rectangular plate with arbitrary boundary conditions based on a higher-order shear deformation theory. *Thin-Walled Structures*, 173, 108930. <https://doi.org/10.1016/j.tws.2022.108930>

Publisher's Note Springer Nature remains neutral with regard to jurisdictional claims in published maps and institutional affiliations.

Springer Nature or its licensor (e.g. a society or other partner) holds exclusive rights to this article under a publishing agreement with the author(s) or other rightsholder(s); author self-archiving of the accepted manuscript version of this article is solely governed by the terms of such publishing agreement and applicable law.